Determination of Fracture Toughness of Epoxy Using Fractography

LUXSAMEE PLANGSANGMAS, JOHN J. MECHOLSKY, JR., ANTHONY B. BRENNAN

Department of Materials Science and Engineering, University of Florida, Gainesville, Florida 32611

Received 26 June 1998; accepted 10 September 1998

ABSTRACT: Fracture toughness of epoxy was determined by quantitative fractography, one of the techniques for brittle materials based on fracture mechanics. Two different epoxy systems, an anhydride-cured and an amine-cured epoxy based upon diglycidyl ether of bisphenol A (DGEBA) were studied. Epoxies with different average molar mass between crosslinks (M_c) or crosslink density were prepared by varying the cure profiles. The materials were characterized using differential scanning calorimetry (DSC), dynamic mechanical spectroscopy (DMS), and density measurements. Optical microscopy was used to measure the dimensions of the different regions on the fracture surfaces of unnotched samples that were tested to failure under tension. The fracture toughness values were calculated from the relationship between the measured sizes and fracture stress. Epoxies with lower M_c values or higher crosslink densities have lower fracture toughness values. © 1999 John Wiley & Sons, Inc. J Appl Polym Sci 72: 257–268, 1999

Key words: epoxy; fracture toughness; fractography; crosslink density

INTRODUCTION

Fracture toughness is a measure of the resistance of a material to propagate cracks. The fracture behavior of a material depends on the stress level, flaw concentration, material properties, and failure mechanism. Different methods and types of specimens are used to determine fracture toughness. They are typically based on the principle of initiating a controlled crack, which will propagate under an applied load, in the specimen. Subsequently, fracture toughness can be calculated from the load-displacement curve and the geometrical constant for each type of specimen. Fracture toughness of epoxies was investigated by several researchers[1–6] using different techniques. Fracture toughness values of epoxies vary over a wide range, that is, 0.4–1.8 MPa $m^{1/2}$, depending on the type of epoxy resin, the curing agent, the stoichiometry of the mix, the cure profile, and the temperature and rate of testing.

Conventional techniques consume much time in the preparation of unique specimen dimensions and shapes and typically require special measuring devices such as a strain gauge for recording precise deflection. Using fractography, fracture toughness can be determined from regular dog-bone samples failed under tension by combining the information from the fracture surfaces and the fracture stress.

Based on linear elastic fracture mechanics (LEFM), Irwin[7] developed a relationship between stress intensity local to the crack and the far-field applied stress and geometry of the structure during loading. Randall[8] reviewed Irwin's analysis, which applied to a flat ellipse with a sharp crack front, embedded in an infinite body, subjected to uniaxial tension normal to the plane of a crack. Mecholsky[9] summarized the equation for K_{IC} (critical stress-intensity factor or fracture toughness in mode I loading) for surface semielliptical cracks of depth a and

Correspondence to: A. B. Brennan.

Contract grant sponsors: National High Magnetic Field Laboratory, Tallahassee, FL; Royal Thai government, Bangkok, Thailand.

Journal of Applied Polymer Science, Vol. 72, 257–268 (1999)

 CCC 0021-8995/99/020257-12

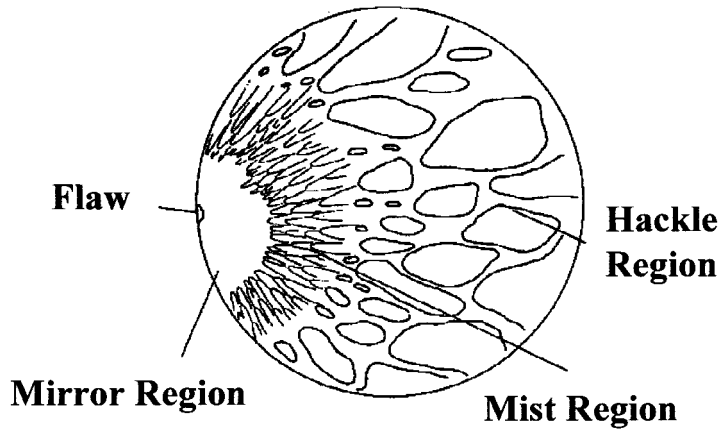

Figure 1 Typical fracture surface of epoxy. Adapted from ref. 11.

half-width, b, which are small relative to the thickness as

$$K_{IC} = 1.1\sigma_f(\pi c)^{1/2}/\phi \quad (1)$$

where σ_f is the stress at fracture; c, either a or b, whichever is smaller (based on the stress distribution at the end of minor axis of the ellipse); and ϕ, an elliptical integral of the second kind which varies between 1 for a slit crack ($a/b = 0$) to 1.57 for $a/b = 1$.

It has been shown[10] that for most glass structures the failure-initiating crack can be modeled as an equivalent semicircular crack of radius c, where $c = (ab)^{1/2}$. By this assumption and by letting $\phi = 1.57$, the equation for K_{IC} can be written as

$$K_{IC} = 1.24\sigma_f\{(ab)^{1/2}\}^{1/2} \quad (2)$$

which will be applied to the analysis of the brittle epoxy materials under investigation.

In some cases, plastic deformation can occur at the crack tip. Assuming that the radius of the plastic zone is small compared to the crack size, LEFM can be applied to the system with some modifications. Randall[8] reviewed Irwin's analysis and showed that

$$(K_{IC})^2 = \{1.2\pi(\sigma_f)^2c\}/[\phi^2 - \{0.212(\sigma_f)^2/(\sigma_{ys})^2\}] \quad (3)$$

where σ_{ys} is the yield stress, which will be applied to the epoxy materials with yield behavior.

General features of the fracture surfaces of epoxies are shown in Figure 1. They are divided into four regions:

1. Initiation region or flaw region: This is the region where fracture has started. The fracture origin normally is due to machining, impact, or material defects such as pores or inclusions. The material defects can be inherent defects that exist naturally in a material or as a consequence of processing.
2. Mirror region: This is an area with a smooth, glossy appearance that surrounds the initiation region. The crack velocity is relatively slow in the mirror region.
3. Mist region: This is an area that appears to be substantially rougher than the mirror region. The crack velocity, which is higher than in the mirror region, creates parabolic or hyperbolic markings in the mist region.
4. Hackle region: The hackle region appears to be the roughest area due to highest crack velocity. Macroscopic crack branching initiates at the end of the hackle region.

Mecholsky[12] made an assessment of quantitative fractography and showed the three important equations for numerical analysis on the fracture surfaces of many brittle materials, which are also composed of four main regions as in epoxies:

$$\sigma c^{1/2} = \text{constant} \quad (4)$$

$$\sigma(r_j)^{1/2} = M_j/Y = K_{Bj} \quad (5)$$

$$c/r_j = \text{constant} \quad (6)$$

where r_j is the radius from the flaw origin to each boundary (r_1 is the mirror region, and r_2, the mist region); σ, the fracture stress; M_j, the constant for

each boundary; c, the critical crack or flaw size; Y, the geometrical constant for the crack shape; and K_{Bj}, the stress intensity at each boundary.

Mecholsky[9] found that in a soda–lime–silica glass M_j and K_{Bj}, by analogy, are constant regardless of whether or not the flaw is in the plane perpendicular to the maximum stress. It was shown that the K_{IC} value is independent of the depth-to-width of the flaw and can be calculated from the mirror constant or stress intensity at each boundary. The ratio of the square root of the depth and width of the flaw to the mirror radius is constant for semielliptical flaws. Mecholsky et al.[13] calculated fracture energies from the mirror data for most glasses over a wide range of composition. The results agreed well with the measured values.

Reed and Walsh[14] studied the tensile properties of epoxy, cyanate ester, vinyl ester, and polyester resin systems at different temperatures and applied the technique of fractography. Their analysis of linear regression plots of the tensile strength and square root of the flaw size showed that at low temperature the sensitivity of the tensile strength to flaw size was twice the sensitivity at room temperature.

The average molar mass between crosslinks (M_c), or crosslink density, which is widely used in the literature to characterize the network structure, can be determined based on the rubber elasticity theory. The network structure must have high enough molar mass and degree of flexibility in order to exhibit rubber elasticity. By assuming that the network will behave as an ideal elastomer when it is above the glass transition or in the rubbery regime, the following equation can be used to calculate M_c:

$$G_r = \Phi \rho RT/M_c \tag{7}$$

when G_r is less than 10^7 Pa and where G_r is the shear modulus in the rubbery regime; Φ, the front factor which is close to unity; ρ, the density; R, the molar gas constant; T, the absolute temperature at which the density was measured; and M_c, the average molar mass between crosslink points.

Commercial epoxies usually have M_c values in the range of 200–400 g/mol which may unlikely have sufficient length to meet the criteria of the rubber elasticity theory. However, experimental results show that the above equation can still be applied to highly crosslinked epoxy materials where $M_c < 1000$ g/mol after considering the non-Gaussian character and finite extensibility of short network chains.[1] From a structure–property point of view, the rubbery modulus of highly crosslinked epoxies is sensitive to small changes in crosslinking. Hence, it can be used to determine the crosslink density of the network and, then, the correlation between the crosslink density and physical properties of the network can be studied.

The relationship between fracture toughness and M_c is still ambiguous. In general, fracture toughness should decrease with decreasing values of M_c since the network structure will be more rigid, a local plastic zone at the crack tip should not be able to develop sufficiently, and it should not be able to dissipate the energy. However, it is difficult to compare the study of M_c and fracture toughness in the literature due to the difference in epoxy composition and cure profile. Levita et al.[15] and van der Sanden and Meijer[16] found that their results agreed with the general trends described above when they varied M_c by using a different molar mass epoxy resin. Truong et al.[17] also found the same results when they varied the cure cycle of the system. On the other hand, Gupta et al.[18] found that fracture toughness reached a maximum at medium crosslink density when they varied the amount of the curing agent. They concluded that in the glassy state not only crosslink density but also intermolecular packing, molecular architecture, the perfection of the network, and overall molar mass affected large-strain properties like fracture toughness, elongation at break, and tensile strength. In the rubbery state, crosslink density seemed to be a more important factor.

Min et al.[19] found that fracture toughness increased with cure temperature until 220°C, then leveled off. The glass transition temperature, which corresponded to crosslink density in this study, also showed the same trend as that of fracture toughness. They concluded that crosslink density was not the predominant factor to determine fracture toughness but that other parameters such as free volume, chain flexibility, and intermolecular packing were more dominant.

Chang and Brittain[20] varied the postcuring time to obtain different crosslink densities of an epoxy system. The results showed the general trend of decreasing fracture toughness with increasing crosslink density for the last 20% extent of curing. In the early stage of curing, that is, the first 80%, the molar mass of the network increases more than does the crosslink density; consequently, fracture toughness should increase with the extent of cure. In the later stage of cur-

ing, the crosslink density of the network increases while the molar mass does not increase much. As a result, fracture toughness should decrease with the extent of cure due to increasing crosslink density.

As described above, the relationship between fracture toughness and crosslink density or M_c is still controversial. No quantitative relationship between the fracture energy or fracture toughness at crack initiation and M_c exists at this time due to the complex fracture behavior. However, Lemay and Kelly[1] found that the fracture energy at crack arrest increased as a function of $M_c^{1/2}$. The composition and cure profile of the epoxy systems mentioned above can be summarized as follows:

Reference	Epoxy System	Cure Profile
1	DGEBA with different molar mass/DDS	200°C, 15 h
15	DGEBA with different molar mass/DDS	180°C, 12 h
16	DGEBA with different molar mass/DDS	Different cure temperature in the range of 120–180°C for 16 h and postcured at 200 or 220°C for 2 h depending on the type of DGEBA
17	DGEBA/piperidine	(1) 60–110°C in 10°C increments at 1-h intervals, then 120°C for 16 h (2) 120°C, 16 h (3) 150°C, 3 h, then 120°C, 16 h (4) 160°C, 6 h, then 120°C, 16 h (5) 160°C, 6 h
18	DGEBA/different amount of mPDA	(1) 75°C, 2 h/125°C, 2 h (2) 75°C, 2 h/125°C, 2 h and postcured at 175°C, 6 h
19	DGEBA/DDS	Different cure temperatures in the range of 160–240°C for 6 h
20	DGEB/DDS	150°C, 2 h, 1 atm N_2, and postcured at 146°C for different times

DGEBA: diglycidyl ether of bisphenol A; DDS: diaminodiphenyl sulfone; mPDA: metaphenylene diamine; DGEB: diglycidyl ether of butanediol.

In summary, M_c alone may not predict the fracture behavior of the network, since the network with the same M_c may exhibit different fracture behavior. DGEBA/mPDA cured with different cure profiles can have very close M_c values but different fracture toughness.[18] The microstructure of the network such as network homogeneity should be investigated carefully before drawing any conclusions on the structure–fracture relationship at initiation.

The goal of this work was to apply fractography to determine fracture toughness (K_{IC}) of two different epoxy systems: an anhydride-cured and an amine-cured epoxy based upon DGEBA. By varying the cure profiles of each epoxy system, epoxies with different M_c or crosslink density can be prepared and the relationship between K_{IC} and M_c can be studied.

EXPERIMENTAL

Materials

Two types of epoxy formulation based upon DGEBA were investigated: One is anhydride-cured, that is, a polyester, that was a commercial epoxy from Composite Technology Development, Inc., and the other is amine-cured, that is, polyamine:

Composition of an Anhydride-Cured Epoxy

Materials	Parts by Weight
A modified liquid epoxide resin	100
A modified dicarboxylic anhydride	90
An aminophenol salt	1.5

Composition of an Amine-Cured Epoxy

Materials	Parts by Weight
Tactix® 123	100
Jeffamine D-230	33

Tactix® 123 is a DGEBA resin from the Dow Chemical Co. Jeffamine D-230 is an amine-curing agent from the Huntsman Co.

Mixing Procedure

The weighed components and 0.1% by weight of Antifoam A were mixed and stirred at room temperature at 350 ± 30 rpm. The mixes were subsequently degassed at 28 in.Hg for approximately 40 min.

Processing Procedure

Aluminum pans [63 mm (diameter) × 17.5 mm] and silicone molds were sprayed with a silicone mold-release agent. The mixture was then cast into aluminum pans to prepare samples for differential scanning calorimetry (DSC), dynamic mechanical spectroscopy (DMS), and density measurement. In addition, the mixture was cast into silicone molds to prepare dog-bone samples (ASTM D638-91, Type I; width of narrow section = 13 mm, length of narrow section = 57 mm, width overall = 19 mm, length overall = 165 mm, distance between grips = 115 mm, radius of fillet = 76 mm).

Curing Procedure

The mixtures were cured in a programmable oven at a heating rate of 0.5°C/min. Cure profiles are as follows:

Cure Profiles of an Anhydride-Cured Epoxy

Cure Profile	Curing Temperature (°C)	Curing Time (h)	Postcuring Temperature (°C)	Postcuring Time (h)
I	110	5	125	8
II	110	5	125	16
III	110	5	125	24

Cure Profiles of an Amine-Cured Epoxy

Cure Profile	Curing Temperature (°C)	Curing Time (h)
I	100	1
II	100	4
III	100	24

Characterization Methods

Dynamic Mechanical Spectroscopy

A Seiko DMS 200 tension-mode analyzer, interfaced with a Seiko SDM/5600H computer, was used to acquire the dynamic mechanical properties of materials described in this study. The instrument was calibrated using the maximum value of the dynamic loss modulus (E'') at 1 Hz for the glass transition temperature of poly(methyl methacrylate) which is 117°C. The elastic response of the instrument was calibrated using tensile modulus of polycarbonate measured at an elongation rate 10%/min in uniaxial tension.

All DMS experiments were performed at the heating and cooling rate of 0.75°C/min, frequency at 0.1, 0.5, 1, 5, and 10 Hz, and the flow rate of dry nitrogen of 200 mL/min. The approximate width and thickness of all samples were 4 and 0.5 mm, respectively. The gauge length was 20 mm for all samples.

Differential Scanning Calorimetry

A Seiko DSC 220C interfaced with a Seiko SDM/5600H computer was used to measure the glass transition of epoxy. The instrument was calibrated for temperature and enthalpy using indium (In), tin (Sn), and bismuth (Bi). The heating rate was 10°C/min and the flow rate of dry nitrogen was 100 mL/min.

All DSC experiments were performed by using an open-type aluminum pan with a crimped flange cover at a heating rate of 10°C/min and the flow rate of dry nitrogen of 100 mL/min. The approximate weight of the samples was 10 mg. Alumina powder was used as the reference. All scans were baseline-corrected using an empty pan. The glass transition temperature was measured as the midpoint of the intersection of the thermal response for the glassy and liquid states. The average glass transition temperature was obtained from the second heat and the third heat of each measurement.

Density Measurement

The density of the epoxy was determined by the displacement method according to ASTM D792-91. The liquid used for displacement was distilled water. Five samples of each cure schedule were measured. The approximate dimension of samples were 10 × 10 × 5 mm. The water adsorption by the epoxy samples was determined, by water-adsorption studies, to be negligible.

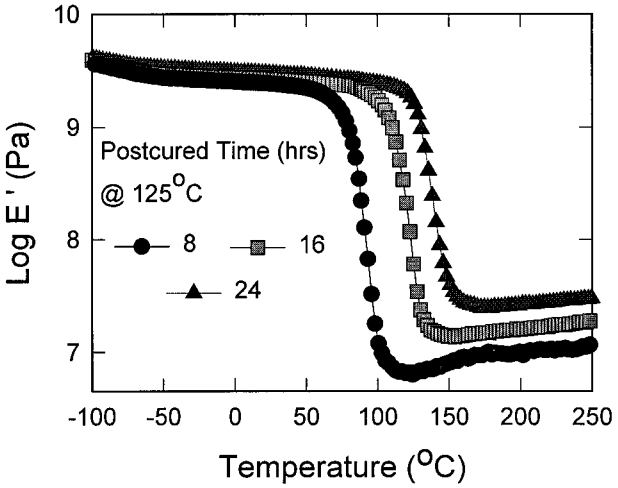

Figure 2 Storage modulus of an anhydride-cured epoxy with different cure profiles. Frequency = 1 Hz; heating rate = 0.75°C/min; N_2 flow rate = 200 mL/min.

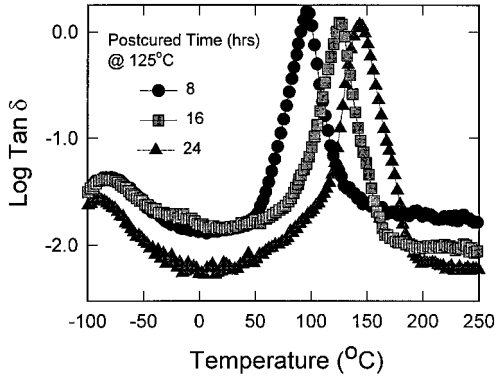

Figure 3 Tan δ relaxation of an anhydride-cured epoxy with different cure profiles. Frequency = 1 Hz; heating rate = 0.75°C/min; N_2 flow rate = 200 mL/min.

Fracture Toughness Determination

Uniaxial Tensile Test at Room Temperature

An Instron universal test instrument (Model 1122) was used to load and fracture the samples in uniaxial tension. The room-temperature stress–strain properties of the epoxy were measured according to ASTM D638M-91. Sample dimensions corresponded to Type I in ASTM D638-91. The approximate thickness was 3 mm and the gauge length was 4.5 in. (115 mm) for all samples. The crosshead speed was 0.5 in. (12.7 mm)/min or 10%/min strain rate for every test. Five to eight samples of each cure schedule were tested except for cure profile III of anhydride-cured epoxy, where only three samples were tested.

Fracture Surface Analysis by Optical Microscopy

Fracture surfaces of each tensile sample were analyzed using an Olympus optical microscope at 50 and 100 magnification. The depth (a) and half-width (b) of fracture-initiating flaws and the radius of the surrounding characteristic topography, that is, mirror, and mist regions on the fracture surfaces, were measured using a reticle. The magnitude of the length was calibrated using a standard glass scale at each magnification. The size of fracture-initiating flaws (c) then were calculated by $c = (ab)^{1/2}$.

RESULTS AND DISCUSSION

Network Characterization

DMS Result

The influence of the cure profile on the thermomechanical properties of the anhydride epoxy is illustrated by the plots of the storage modulus (E') and tan δ versus temperature (Figs. 2 and 3). As expected, the crosslink density, as indicated by the peak temperature of the tan δ, reached a maximum using the cure profile III. The influence of the cure profile was not as significant in the amine-based epoxy as illustrated by the plots of the storage modulus (E') and tan δ versus temperature (Figs. 4 and 5). This is due to the kinetics of the polymerization of the amine-curing agent (Jeffamine D-230). De Nograro et al.[21] studied the effect of the chemical structure of the curing agent on the curing evolution of different epoxy systems. They found that the gelation time of DGEBA epoxy cured with Jeffamine D-230 at a stoichiometric ratio was 38, 85, 216, and 435 min at curing temperatures of 70, 60, 50, and 40°C, respectively. Therefore, it was reasonable that there would be minimal differences associated

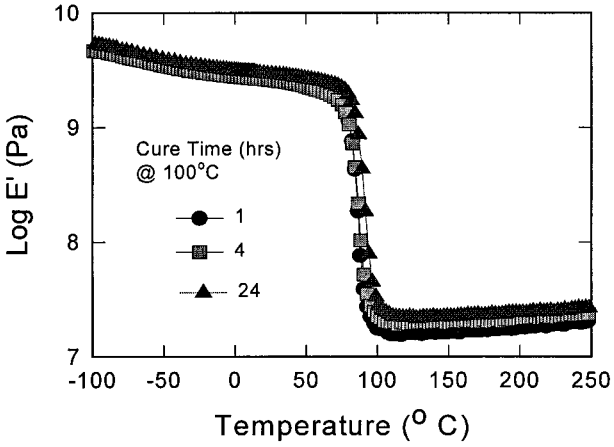

Figure 4 Storage modulus of an amine-cured epoxy with different cure profiles. Frequency = 1 Hz; heating rate = 0.75°C/min; N_2 flow rate = 200 mL/min.

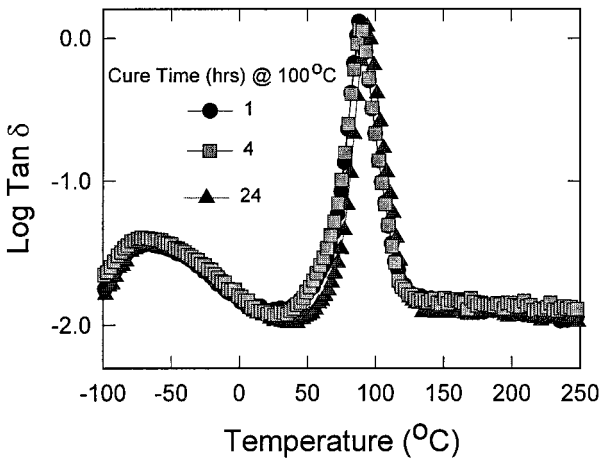

Figure 5 Tan δ relaxation of an amine-cured epoxy with different cure profiles. Frequency = 1 Hz; heating rate = 0.75°C/min; N_2 flow rate = 200 mL/min.

with the cure profile for the amine-cured epoxy in our study.

Glass Transition Temperature

The influence of the cure profile on the glass transition temperature of the anhydride-cured epoxy is shown in Table I. As expected, the epoxy with cure profile III, which has the maximum crosslink density, exhibits the highest T_g. The influence of the cure profile on the glass transition temperature of the amine-cured epoxy is shown in Table II. The epoxy with cure profile III exhibits the highest T_g (86.6°C). Lee and McKenna[22] studied the same amine-cured epoxy with the same cure profile and determined the T_g from DSC = 87.3°C, which is close to the value from this study. However, the glass transition temperature of the epoxies with cure profiles I, II, and III do not significantly differ from each other due to the kinetics of the polymerization of the amine-curing agent (Jeffamine D-230) as described above. The

Table I Glass Transition Temperature of Anhydride-Cured Epoxy

Cure Profile	T_g from DSC[a] (°C)	T_g from max E'' [b] (°C)	T_g from max tan δ[b] (°C)
I	91.7 ± 1.1	76.3	97.0
II	113.5 ± 1.9	102.1	115.6
III	138.4 ± 1.8	129.1	143.5

[a] Rate of heating and cooling = 10°C/min.
[b] Rate of heating and cooling = 0.75°C/min.

Table II Glass Transition Temperature of Amine-Cured Epoxy

Cure Profile	T_g from DSC[a] (°C)	T_g from max E'' [b] (°C)	T_g from max tan δ[b] (°C)
I	84.0 ± 0.1	79.5	88.1
II	83.8 ± 0.3	78.5	89.4
III	86.6 ± 0.5	83.9	94.1

[a] Rate of heating and cooling = 10°C/min.
[b] Rate of heating and cooling = 0.75°C/min.

temperature at the maximum damping or tan δ at 1 Hz is generally 15–20°C above the T_g from DSC and the temperature of the maximum loss modulus at low frequency can be defined as the T_g.[23] In this study, the temperature of the maximum loss modulus at 1 Hz is used as the T_g for determining the rubbery modulus at T_g + 50°C. We also consider the difference in the heating rates using DSC and DMS, which are 10 and 0.75°C/min, respectively. Epoxy in DMS will have more time at the curing temperature and above than in DSC. Therefore, the network may be activated and additional crosslinking may occur. However, we assume that this additional crosslinking will be the same for the same heating rate. T_g values determined from the DSC curves, T_g values approximated from the temperature of maximum loss modulus, and T_g values approximated from the temperature of maximum damping or tan δ exhibit the same trend for both anhydride-cured epoxy and amine-cured epoxy. Much work[15,24–26] has been done on different epoxy systems and these studies found the same trend, that is, epoxy with a higher crosslink density or lower M_c will have a higher T_g.

Density Results

The densities of anhydride-cured epoxy and amine-cured epoxy are shown in Tables III and IV, respectively. The mean values of the density

Table III Density of Anhydride-Cured Epoxy at Room Temperature

Cure Profile	Density (g/cm^3)[a]
I	1.228 (0.0006)
II	1.226 (0.0008)
III	1.218 (0.0004)

[a] Value in parentheses = 1 standard deviation.

Table IV Density of Amine-Cured Epoxy at Room Temperature

Cure Profile	Density (g/cm^3)[a]
I	1.156 (0.0007)
II	1.156 (0.0005)
III	1.155 (0.0003)

[a] Value in parentheses = 1 standard deviation.

of both epoxies are not statistically different at $\alpha = 0.5$ by the one-way analysis of variance. There are disagreements in the literature on the effect of the extent of the cure or crosslink density in epoxy on the density. Noordam et al.[27] studied different epoxy systems and found that the density measured at room temperature could remain constant, increase, or decrease with respect to the extent of cure depending on each network system. They suggested that density was not a good measure of the free volume since the effect of chemical shrinkage at the curing temperature and/or the increase in T_g could compensate for the increase of the free volume. Morgan et al.[26] found the trend of decreasing density with increasing crosslink density. On the other hand, Chang et al.[24] and Fisher[25] found that the density of epoxy increased with the extent of cure due to decrease in the free volume of epoxy with higher crosslink density.

Calculation of M_c

M_c was calculated by assuming that $G'_r = E'_r/3$, where G'_r is the shear modulus in the rubbery regime and E'_r is the tensile modulus in the rubbery regime. E'_r was determined from E' at T_g + 50°C from the DMS result at 1 Hz. As shown in Tables V and VI, M_c decreases with curing time for both anhydride-cured epoxy and amine-cured epoxy as found by Chang et al.[24]

Fracture Toughness Determination

Uniaxial Tensile Test at Room Temperature

Tensile properties of anhydride-cured epoxy and amine-cured epoxy are shown in Tables VII and VIII, respectively. Anhydride-cured epoxy exhibits brittle behavior; no obvious yielding occurs. On the other hand, amine-cured epoxy exhibits yielding before fracture.

Table V M_c of Anhydride-Cured Epoxy

Cure Profile	M_c (g/mol)
I	1394
II	617
III	364

Table VI M_c of Amine-Cured Epoxy

Cure Profile	M_c (g/mol)
I	539
II	444
III	388

Relationship Between K_{IC} *and* M_c

The plot of K_{IC} versus M_c of anhydride-cured epoxy and amine-cured epoxy is illustrated in Figure 6. Anhydride-cured epoxy shows that K_{IC} increases with an increase in M_c or a decrease in crosslink density. The mean values of K_{IC} of anhydride-cured epoxy are 1.31, 1.12, and 0.98 MPa m$^{1/2}$ for cure profiles I, II, and III, respectively. They are statistically different at $\alpha = 0.5$ by the one-way analysis of variance. The mean values of K_{IC} of amine-cured epoxy are 1.40, 1.47, and 1.24 MPa m$^{1/2}$ for cure profiles I, II, and III, respectively. They are not statistically different at $\alpha = 0.5$ by the one-way analysis of variance. They may have the same K_{IC}. As shown in Figure 6, we cannot compare different epoxy systems using M_c as a parameter. Anhydride-cured epoxy with an M_c of 1394 g/mol still has a lower K_{IC} than does amine-cured epoxy with an M_c of 444 g/mol. The relationship between K_{IC} and M_c depends much on the fracture mechanism of each epoxy system during crack initiation.

Relationship Between Fracture Stress and Sizes of Different Regions on Fracture Surface

The plots of fracture stress versus 1/(flaw size)$^{1/2}$ of anhydride-cured epoxy are illustrated in Figure 7. The data points of anhydride-cured epoxy with

Table VII Tensile Properties of Anhydride-Cured Epoxy

Cure Profile	Tensile Strength (MPa)	Elongation at Break (%)	Young's Modulus (GPa)
I	62.9 ± 6.0	2.63 ± 0.31	2.71 ± 0.19
II	69.4 ± 10.7	2.98 ± 0.39	2.78 ± 0.11
III	83.2 ± 3.6	3.13 ± 0.20	2.91 ± 0.13

Table VIII Tensile Properties of Amine-Cured Epoxy

Cure Profile	Offset Yield Strength (MPa) at 0.2% Elongation	Tensile Strength (MPa)	Elongation at Break (%)	Young's Modulus (GPa)
I	50.01 ± 3.28	63.2 ± 2.08	3.76 ± 0.45	2.63 ± 0.04
II	43.51 ± 3.18	62.2 ± 1.93	4.43 ± 0.78	2.57 ± 0.07
III	46.06 ± 0.61	59.7 ± 2.07	3.94 ± 0.18	2.82 ± 0.06

cure profile II lie closer to the dashed line, which was calculated from the average K_{IC}. The general trend of the plot comes from eq. (2). The data should follow a straight line with the slope of $K_{IC}/1.24$.

The plots of fracture stress versus 1/(mirror radius)$^{1/2}$ of anhydride-cured epoxy and amine-cured epoxy are illustrated in Figures 8 and 9. The dashed lines were calculated from the average mirror constant for the mirror region of each cure profile. The plot should be a straight line with the slope equal to the mirror constant if their failure behavior is the same as that of glass. But the results are so scattered that we cannot draw any conclusions. However, it can be noticed that anhydride-cured epoxy with cure profile I has a different slope from that of cure profile II.

The plots of flaw size versus mirror radius of anhydride-cured epoxy and amine-cured epoxy are illustrated in Figures 10 and 11. The dashed lines were calculated from the average mirror-to-flaw size ratio for each cure profile. The plot should be a straight line based on the fracture behavior of glass. The same trend was found as that in Figures 8 and 9.

Fracture Surface Analysis by Optical Microscopy

Fracture surfaces of anhydride-cured epoxy and amine-cured epoxy are illustrated in Figures 12 and 13, respectively. Fracture surfaces of both materials exhibit four regions, that is, fracture-initiating flaw, mirror region, mist region, and hackle region as those that appeared in typical epoxies. The close-end of parabolic markings in the mist or hackle region will point to the origin of the flaw. General cracks will propagate from the origin of the flaw. However, some small cracks within the parabolas will propagate in the opposite direction of the general crack path. Air bubbles, inclusions, and cracks are three types of flaws found in this study. Most of them were surface flaws. Air bubbles caused some difficulties in finding the origin and measuring the flaw size. In this study, the flaw size that originated from a bubble was the radius of the bubble. The main difference in the feature of fracture surfaces of both epoxies is the crack arrest line. Anhydride-cured epoxy shows no evidence of crack arrest lines, whereas amine-cured epoxy shows crack arrest lines across the markings from the origin of the flaw. Amine-cured epoxy appears to have more plas-

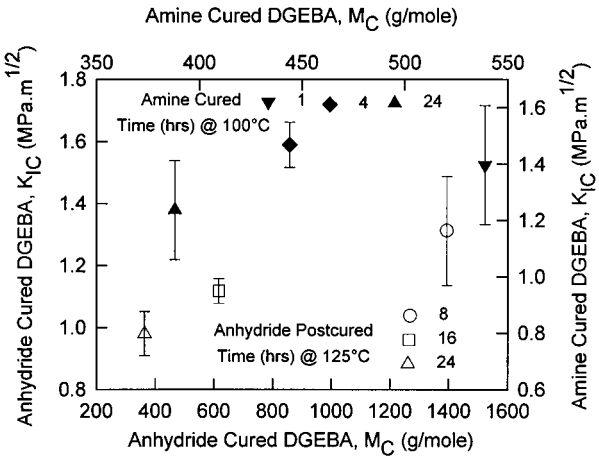

Figure 6 K_{IC} at room temperature as a function of M_c for an anhydride- and an amine-cured epoxy with different cure profiles.

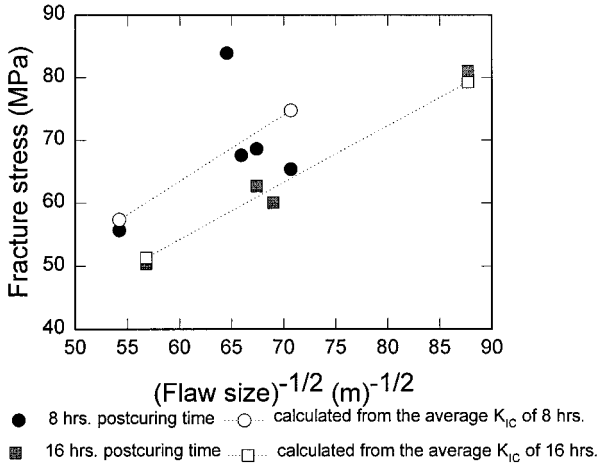

Figure 7 Fracture stress and inverse of square root of flaw-size relationship for an anhydride-cured epoxy with different cure profiles.

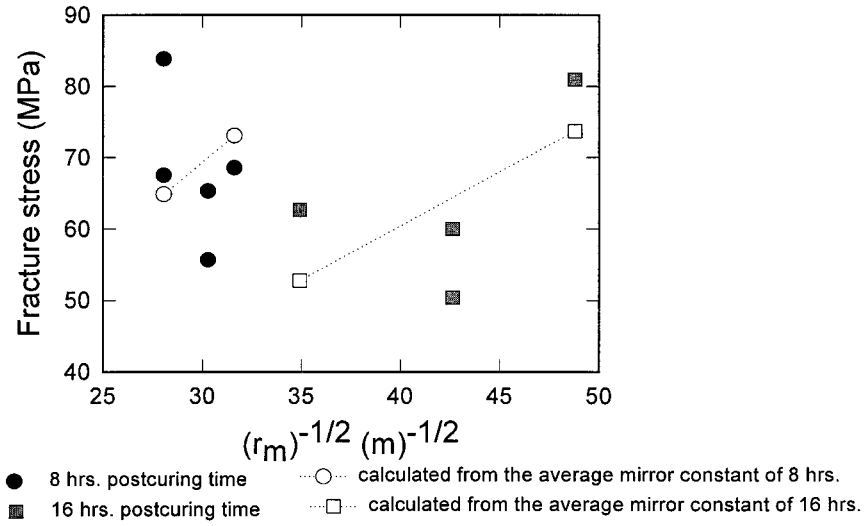

Figure 8 Fracture stress and inverse of the square root of the mirror radius relationship for an anhydride-cured epoxy with different cure profiles.

tic deformation than has anhydride-cured epoxy according to their stress–strain behavior. Therefore, local plastic deformation can develop at the crack tip, which can be an obstacle for crack propagation. Cracks will then arrest and change their direction. Phillips et al.[28] also found the same pattern of crack arrest lines in the amine-cured epoxy.

CONCLUSIONS

According to the network characterization results, anhydride-cured epoxy shows a significant difference in the network structure among three cure profiles. The system is not fully cured; further crosslinking can occur for longer postcuring time. The results show the trend to agree with the hypothesis, that is, K_{IC} decreases with decreases in M_c or increases in postcuring time. Their mean values are statistically different at $\alpha = 0.05$ by the one-way analysis of variance. On the other hand, amine-cured epoxy does not show a significant difference in the network structure because the system is almost fully cured after 1 h. There is not much further crosslinking after 1 h; K_{IC} should not be much different. Their mean values

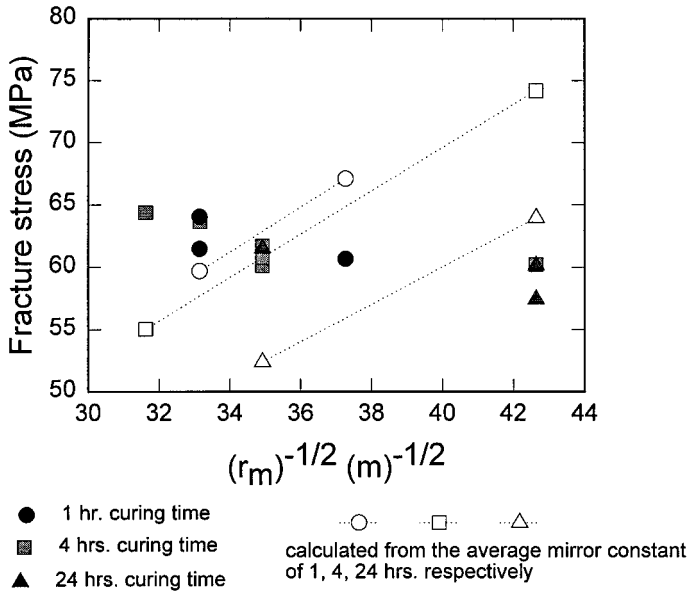

Figure 9 Fracture stress and inverse of the square root of the mirror radius relationship for amine-cured epoxy with different cure profiles.

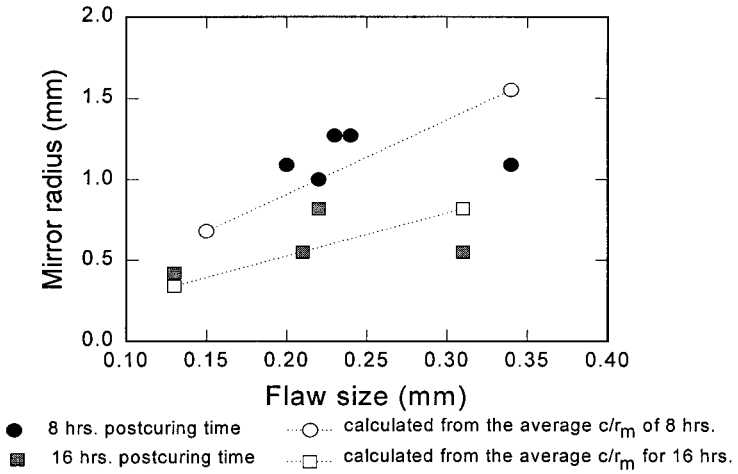

Figure 10 Mirror radius and flaw-size relationship for an anhydride-cured epoxy with different cure profiles.

are not statistically different at $\alpha = 0.05$ using the one-way analysis of variance. However, the K_{IC}'s for both epoxies are still in the range of most epoxies. The features on the fracture surface appear similar to glass. Anhydride-cured epoxy does not show distinct crack arrest lines on fracture surfaces as amine-cured epoxy does. This can be explained by the difference in yielding behavior between these two epoxies. The mirror constant and flaw-to-mirror ratio results of anhydride-cured epoxy with different cure profiles seem to be different from each other, whereas the mirror constant and flaw-to-mirror ratio results of amine-cured epoxy with different cure profiles seems to lie close to each other.

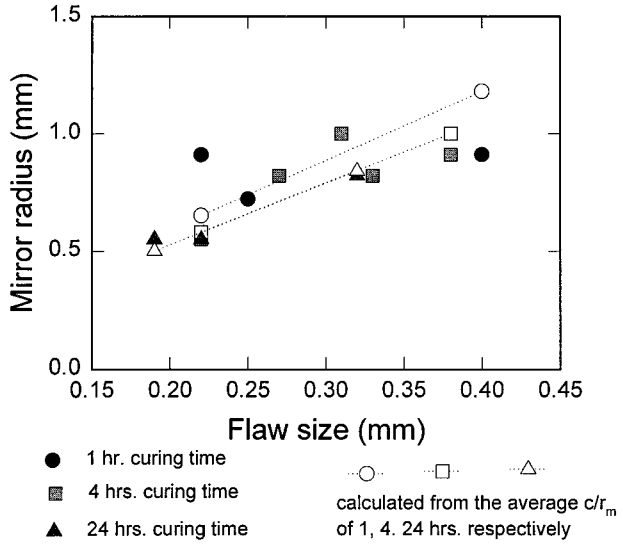

Figure 11 Mirror radius and flaw-size relationship for an amine-cured epoxy with different cure profiles.

It is suggested that fractography could be a reliable technique for determining the K_{IC} of brittle polymers and polymers with small plastic deformation by accounting for some corrections. A larger population size should help in interpreting the results or drawing conclusions. In the case of a polymer with some plastic deformation, K_{IC} should be compared to a different method, for example, compact tension or double torsion, in order to confirm the validity of this technique.

The relationship between K_{IC} and M_c agrees with the general trend but it is not a simple linear relation. Other factors such as chemical structure and network homogeneity contribute as well to K_{IC}.

It would be better if both inherent and processing defects could be eliminated as much as possible. Purifying or warming epoxy resin before mixing will reduce inherent defects such as inclusions. Ad-

Figure 12 Fracture surface of an anhydride-cured epoxy with a crack and parabolic markings. Optical micrograph at 50×.

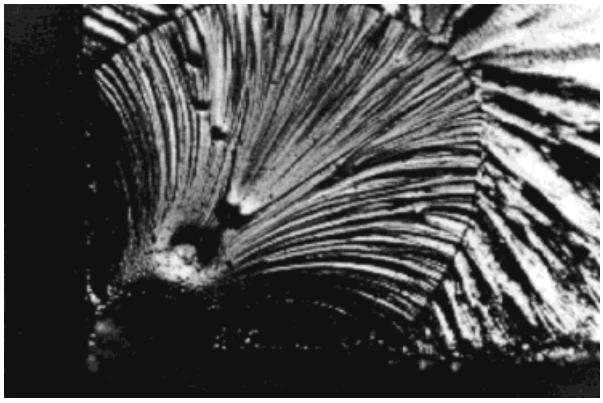

Figure 13 Fracture surface of amine-cured epoxy with a bubble and crack arrest lines. Optical micrograph at 50×.

vanced degassing techniques or casting in a big sheet before machining dog-bone samples will also reduce processing defects such as bubbles.

REFERENCES

1. LeMay, J. D.; Kelly, F. N. in Advances in Polymer Science 78; Springer-Verlag: Berlin, 1986; pp 115–148.
2. Yamini, S.; Young, R. J. Polymer 1977, 18, 1075.
3. Kinloch, A. J.; Williams, A. J. J Mater Sci 1980, 15, 987.
4. Young, R. J.; Beaumont, P. W. R. J Mater Sci Lett 1976, 11, 776.
5. Hollmann, K.; Hahn, H. T. Polym Eng Sci 1989, 29, 523.
6. Yamini, S.; Young, R. J. J Mater Sci 1980, 15, 1823.
7. Irwin, G. W. Trans ASME J Appl Mech 1962, 29, 651.
8. Randall, P. N. in ASTM STP 410, 1967; pp 88–126.
9. Mecholsky, J. J. in Experimental Technique of Glass Science; American Ceramic Society: Westerville, OH, 1993; pp 483–520.
10. Mecholsky, J. J.; Freiman, S. W.; Rice, R. W. J Am Ceram Soc 1977, 60, 114.
11. Cantwell, W. J.; Roulin-Moloney, A. C. Fractography and Failure Mechanisms of Polymers and Composites; Elsevier: London, 1989; p 252.
12. Mecholsky, J. J. in Ceramic Transactions; Vol. 17, Fractography of Glass and Ceramics II; American Ceramic Society: Westerville, OH, 1991; pp 413–452.
13. Mecholsky, J. J.; Rice, R. W.; Freiman, S. W. J Am Ceram Soc 1977, 57, 440.
14. Reed, R. P.; Walsh, R. P. Adv Cryo Eng 1994, 40, 1129.
15. Levita, G.; de Petris, S.; Marchetti, A.; Lazzeri, A. J Mater Sci 1991, 26, 2348.
16. van der Sanden, M. C. M.; Meijer, H. E. H. Polymer 1993, 34, 5063.
17. Truong, V. T.; Truong, Y. B.; Ennis, B. C. Polym Commun 1991, 32, 275.
18. Gupta, V. B.; Drzal, L. T.; Lee, C. Y-C.; Rich, M. J. Polym Eng Sci 1985, 25, 812.
19. Min, B.-G.; Hodgkin, J. H.; Stachurski, Z. H. J Appl Polym Sci 1993, 48, 1303.
20. Chang, T. D.; Brittain, J. O. Polym Eng Sci 1982, 22, 1228.
21. de Nograro, F. F.; Guerrero, P.; Corcuera, M. A.; Mondragon, I. J Appl Polym Sci 1995, 56, 177.
22. Lee, A.; McKenna, G. B. Polymer 1988, 29, 1812.
23. Nielsen, L. E.; Landel, R. F. Mechanical Properties of Polymers and Composites; Marcel Decker: New York, 1994.
24. Chang, T. D.; Carr, S. H.; Brittain, J. O. Polym Eng Sci 1982, 22, 1213.
25. Fischer, M. in Advances in Polymer Science 100; Springer-Verlag: Berlin, 1992; pp 313–355.
26. Morgan, R. J.; Kong, F. M.; Walkup, C. M. Polymer 1984, 25, 375.
27. Noordam, A.; Wintraecken, J. J. M. H.; Walton, G. in Crosslinked Epoxies; Walter de Gruyter: Berlin, 1987; pp 373–389.
28. Phillips, D. C.; Scott, J. M.; Jones, M. J Mater Sci 1978, 13, 311.